NANOSYSTEMS:
PHYSICS, CHEMISTRY, MATHEMATICS

Klimonsky S.O., et al. *Nanosystems: Phys. Chem. Math.*, 2024, **15** (6), 902–909.
http://nanojournal.ifmo.ru
DOI 10.17586/2220-8054-2024-15-6-902-909

Original article

SERS substrates based on opal films with gold coating

Mikhail O. Astafurov[1], Elena V. Perevedentseva[2], Nikolay N. Melnik[2], Alexander E. Baranchikov[3], Sergey G. Dorofeev[1], Alexander A. Ezhov[1], Anastasia V. Grigorieva[1], Sergey O. Klimonsky[1]

[1]Lomonosov Moscow State University, Moscow, Russia

[2]P. N. Lebedev Physical Institute of the Russian Academy of Sciences, Moscow, Russia

[3]Kurnakov Institute of General and Inorganic Chemistry of the Russian Academy of Sciences, Moscow, Russia

Corresponding author: Sergey O. Klimonsky, klimonskyso@my.msu.ru

ABSTRACT Substrates for Surface-Enhanced Raman Spectroscopy (SERS) were fabricated by gold sputtering onto surface of synthetic opal films and their characteristics were studied at wavelengths $\lambda = 532$ and 785 nm. Synthetic opal films were fabricated by self-assembly of spherical SiO_2 particles on vertical substrates. It was found that at the concentration of the analyte methylene blue equal to 10^{-5} M the intensity of SERS at the wavelength of 785 nm increased with increasing amount of sputtered gold up to a certain optimal thickness exceeding 35 nm, while at the concentration of 10^{-6} M this dependence was not observed. It is assumed that this is due to the complex amount-dependent morphology of the sputtered gold coating and the presence of "hot spots" of different strengths. For the best samples at a wavelength of $\lambda = 785$ nm, the SERS enhancement factor was of $7 \cdot 10^4$ and a detection limit for methylene blue reached $3 \cdot 10^{-7}$ M that exceeds the results published for similar substrates previously. The SERS parameters obtained for $\lambda = 532$ nm were less attractive, despite the additional enhancement due to this wavelength was at the edge of the photonic stop-band.

KEYWORDS silica opal, gold coating, Surface-Enhanced Raman spectroscopy

ACKNOWLEDGEMENTS The authors are grateful to the Russian Science Foundation for financial support of the present research (Grant No. 23-23-00252). This work was partially performed using the scanning probe microscope NT-MDT NTEGRA Prima upgraded up to NT-MDT NTEGRA II by Nova SPb from Program for the Development of Moscow State University. Scanning electron microscopy was performed using the equipment of the JRC PMR IGIC RAS. The authors also thank Daniil Kozlov for assistance with electron microscopy.

FOR CITATION Astafurov M.O., Perevedentseva E.V., Melnik N.N., Baranchikov A.E., Dorofeev S.G., Ezhov A.A., Grigorieva A.V., Klimonsky S.O. SERS substrates based on opal films with gold coating. *Nanosystems: Phys. Chem. Math.*, 2024, **15** (6), 902–909.

1. Introduction

Surface-Enhanced Raman Spectroscopy (SERS) is one of the most promising branches of optical spectroscopy. Research in this field is mainly aims to create new materials (SERS substrates) that would have high Raman enhancement factor (*EF*) and low detection limit in combination with reproducibility of their properties, uniformity, stability and manufacturability. The key point here is the creation of so-called "hot spots" between metal nanoparticles or on nanoscale features of topography of the metal surface. The electromagnetic field in hot spots at the frequency of the light wave is to be as strong as possible, and the number of molecules of the detected compound (analyte) should be as large as possible.

In recent years, several different approaches have been proposed to create SERS substrates with record high characteristics based on the uniform distribution of silver nanoparticles on the substrate surface [1, 2], creation of a monolayer of silver nanoparticles on the surface of multilayer metal-dielectric structures [3], using films of silver inverse opals [4], as well as inverse opals decorated with various gold or silver nanoparticles [5, 6], construction of honeycomb gold nanostructures [7], silver wrinkles with gold nanoparticles lined at the tips [8], sputtering of silver on polydimethylsiloxane substrates with nanopits [9], etc. Despite the impressive results achieved in some of these works (a detection limit of the order of 10^{-20} M was achieved in [8], for example), in most cases the described technologies are rather complicated and have not been confirmed by other authors. At the same time, there is still a steady interest in simpler methods which although do not give record-breaking performance are characterized by good manufacturability and high reproducibility of the properties of the obtained SERS substrates. In particular, such methods include the use of noninverted opal-type films on which silver or gold is sputtered on top [10–14]. It is assumed that hot spots in this case can arise in places where the spheres forming the opal film are in contact with each other [10, 13, 14].

Responsible for the large electric field strength in such hot spots are plasmons localized in the metal layers around the contact points of neighboring spheres [13]. In most cases [11–14], silver has been used for sputtering. In the best works of this type [13,14], the surface morphology was further complicated by the addition of polystyrene spheres of small

diameter [13] or the thermal conversion of the silver layer into nanoparticles [14]; a SERS enhancement factor of about $1 \cdot 10^8$ and a rhodamine 6G detection limit of about 10^{-14} [13] or 10^{-13} M [14] were obtained. Gold may be more attractive due to its high chemical stability, but we are aware of only one work on the SERS [10] in which it was used for sputtering onto a silica opal film. In this work a 5 nm thick gold coating was deposited by electron beam evaporation. No explanation as to why this particular thickness was chosen was given by the authors. The detection limit of rhodamine 6G was obtained in the order of $1 \cdot 10^{-6}$ M in the case when the photonic stop band normal to the opal film coincided with the wavelength of the SERS laser, and it was of $1 \cdot 10^{-5}$ M when there was no such coincidence. No estimates of the *EF* were given in Ref. [10].

Note that the influence of the photonic stop band is due to the slow photon effect inside photonic crystal (see reviews [15, 16]). In the case of SERS, the additional enhancement factor due to this effect can be more than one order of magnitude [17]. The synergistic effect between SERS and photonic stop band was reported not only in [10] but also in [11, 12]. In these studies, very thin (5 nm in [10, 12]) or island-like [11] metal coatings were used. However, this effect was not mentioned in [13], where a silver thickness of 80 nm was established as optimal. Obviously, in the latter case, light passes poorly through the metal layer and cannot effectively interact with the photonic crystal. Thus, a dilemma arises whether it is necessary to optimize the metal thickness to achieve maximum plasmon-assisted SERS or to reduce it as much as possible to obtain additional enhancement due to the photonic stop band.

In the present work, we performed a more detailed study of the SERS activity of gold-coated opal films. We collected data on the influence of the amount of sputtered gold on the properties of Au/SiO_2 opal composite, estimated the *EF* and obtained a better detection limit compared to [10]. The influence of the photonic stop band is also discussed.

2. Experimental methods

Films with opal structure were obtained using a vertical deposition self-assembly process using a colloid of SiO_2 spheres [18]. Fine-distribution SiO_2 particles with diameter of about $D \approx 250$ nm were prepared by seeded growth from nanosized nuclei [19], which were obtained by Stöber method [20]. Growing up of nuclei was provided by dropping of additional tetraethyl orthosilicate (TEOS, 99 %, Sigma-Aldrich) to the reactionary vessel performed every 10 mins according to the scheme described in Ref. [19]. Properties of the films prepared are presented in Refs. [19,21]. Sputtering of gold was carried out by thermal evaporation of metal gold (99.9 %, Sberbank) using a PVD coating machine VUP-5 equipped with a direct expansion molybdenum evaporator at a pressure of 10^{-5} torr. Amount of gold deposited was controlled with a precision of ± 7 % using the samples of even gold coatings on bare glass substrates by atomic-force microscopy (AFM). To determine a thickness of the gold coating d it was partly removed in specially formed grooves, the depth of groves was examined by atomic-force microscope NT-MDT NTEGRA Prima modernized by Nova SPb company up to the level of NT-MDT NTEGRA II. A thickness of gold coating d was varied in different experiments from 12 to 100 nm (Table 1).

TABLE 1. Parameters and properties of the studied samples

The sample number	d, nm	S, mm^2		SERS Enhancement Factor*	
		10^{-5} M	10^{-6} M	$\lambda = 785$ nm	$\lambda = 532$ nm
1	12	12 ± 1	8.3 ± 0.3	$9 \cdot 10^3$	$1.4 \cdot 10^3$
2	16	12 ± 1	8.3 ± 0.3	$2 \cdot 10^4$	$0.8 \cdot 10^3$
3	34	19 ± 1	8.3 ± 0.3	$7 \cdot 10^4$	$1 \cdot 10^4$
4	100	23 ± 1	—	$5 \cdot 10^3$	—

S – area of deposited droplets of the analyte (MB),

d – the thickness of gold coating at the test substrates.

*SERS *EF* was estimated for the concentration of analyte of $C = 10^{-5}$ M.

Before the SERS experiment 5 μl droplets of aqueous solutions of methylene blue (MB, 99 %, LLC "Nasklade") with concentrations from $C = 10^{-5}$ to $C = 10^{-7}$ M were deposited to the top of samples with gold coatings. The surface area of droplets varied from 8 to 19 mm^2 (see Table 1). Variation of the surface area of the droplets originated from using of different pipettes for analyte deposition. We did not find any evident effect of thickness of a gold coating on droplet spreading and its final surface area. The surface area of droplets was taken into account when compared intensities of SERS peaks and *EF*s. Measurements of Raman scattering of a model analyte methylene blue (MB) were performed after the droplets were dried completely. SERS spectra were averaged using 4 – 6 randomly selected points. Typical standard

deviations of the intensities of the obtained MB peaks over a sample were ± 15 – 17 %. As a reference sample for further calculating the *EF*, a quartz glass plate with a drop of MB with a concentration of $C_0 = 0.08$ M was used.

All the samples were characterized with a high resolution scanning electron microscope with a field emission cathode (SEM) Carl Zeiss NVision 40, and a scanning spectrophotometer Perkin-Elmer Lambda 950. SERS spectra were collected using Renishaw InVia Raman Microscope with laser emission wavelengths $\lambda = 785$ and 532 nm (average power 45 and 25 mW, laser spot diameter 1 and 3 μm, respectively), equipped with long focal length lens Leica N Plan 50/0.50. Attenuation filters of 0.1 and 1 % were used for 785 and 532 nm lasers, respectively, with an accumulation time of 100 s in all cases.

3. Results and discussion

We examined four samples that differed in the amount of sputtered gold (Table 1). SEM images of the first three of these samples are shown in Fig. 1. As can be seen, the morphology of the gold coating changes at a thickness of $d \approx 15$ nm. At lower thickness, gold forms a non-continuous film with branched narrow grooves on the surface of SiO_2 spheres (Fig. 1a). The characteristic lateral size of continuous parts was approximately of 100 – 150 nm. On the contrary, at greater thickness it covers them with a continuous layer, but between SiO_2 particles there still remain gaps and channels not filled with gold even in this case (Fig. 1, panels b and c). It is interesting to note that the formation of non-continuous silver coating of "island-like metal particles" of approximately the same size (125 – 150 nm) was also reported in Ref. [11]. The composites were synthesized by sputtering small amounts of silver on silica opal films ($D = 242$ nm), and such coatings showed the highest SERS spectra intensity for methylene blue (MB).

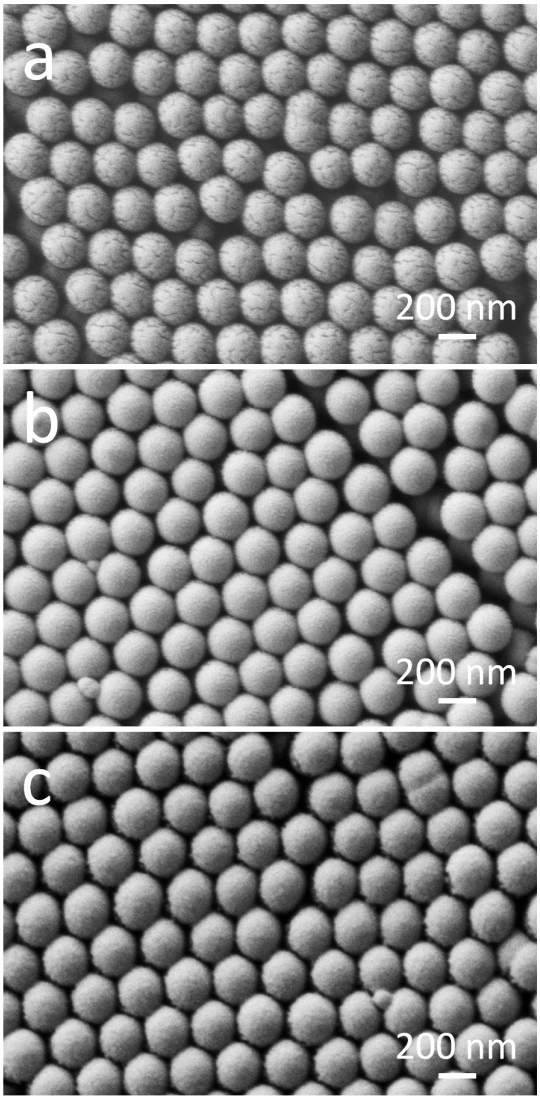

FIG. 1. SEM images of the surface of samples with different amounts of sputtered gold. Thickness of the gold film d on the corresponding bare glass plates were as following: a – 12 nm, b – 16 nm, c – 34 nm (samples 1, 2 and 3 from Table 1, respectively)

The specular reflectance spectra for all three samples are shown in Fig. 2. At both longer and shorter wavelengths, the reflectance increases with increasing amount of sputtered gold. A different sequence of curves is observed around 540 nm, where the photonic stop band is located. With increasing amount of gold, the associated reflectance maximum decreases as less light passes through the gold coating and enters deep into the film. As a result, the reflection from the film with $d = 34$ nm (see curve 3) appears to be less in this region than the others.

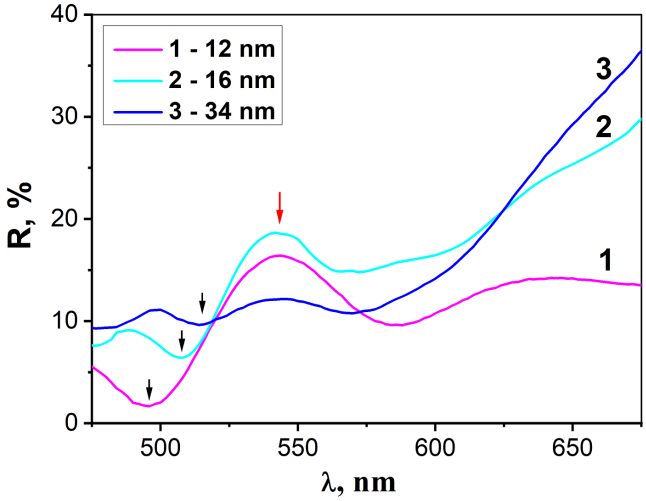

FIG. 2. Specular reflectance spectra at the angle 8° for samples with different amounts of sputtered gold. The numbers of curves correspond to the numbers of samples in Table 1

To the left of the maximum in all three curves (Fig. 2), there is a minimum, marked by black arrows, which is natural to associate with plasmon resonance. These may be plasmons localized on the protrusions and pits on the gold coating. As the thickness of the coating increases, its topography becomes smoother, and, accordingly, the plasmon resonance shifts toward longer wavelengths. It is remarkable that this plasmon resonance effect is not relevant to the SERS spectra at wavelength $\lambda = 785$ nm. Probably, the SERS effect could be associated in this case with far-away plasmons whose spectrum can be much broader than the minima marked by black arrows in Fig. 2.

Figure 3 shows the SERS spectra collected at a wavelength $\lambda = 785$ nm at different concentrations of MB in droplets. It is noticeable that at $C = 10^{-5}$ M the height of the strongest peak at about 1622 cm^{-1} (the C – C stretching mode of toluene ring) increases significantly with increasing amount of sputtered gold, while at MB concentration of $C = 10^{-6}$ M the changes are less significant and the maximum height is obtained for the sample with gold coating thickness of 16 nm. The changes in the height of this peak as a function of the sputtered gold thickness d are shown in Fig. 4. We took into account that the intensity of the SERS modes depends on the number of analyte molecules per a unit area of the substrate. This amount is inversely proportional to the area of the droplets, so for a more correct comparison in Fig. 4 the height of the SERS peak is multiplied by the droplet area S, namely, in Fig. 4 the "height $\times S$" is plotted vertically. The plotted values are also normalized to one for $d = 12$ nm. By the way, the droplet area (see Table 1) has a significant effect on the position of the points in Fig. 4 for $d = 34$ nm at $C = 10^{-5}$ M.

Most likely, the peak at 957 – 970 cm^{-1} in Fig. 3 is not related to the spectrum of the analyte. It increased with a growth of gold coating thickness and was significant in spectra of MB at concentration of 10^{-6} M only, while the strongest maximum at 1622 cm^{-1} became less intensive. Most likely, this peak originated as vibration modes of substrates.

The different character of the dependences in Fig. 4 is related, in our opinion, to the complex structure of the gold coatings which cover silica opal films. At low concentrations of the MB dye, it apparently enters the nanopores and grooves of gold where weak SERS hot spots could be formed. At small thicknesses of the gold coatings, the dye, most likely, is also there even at a concentration of $C = 10^{-5}$ M. In this case, the ratio between the height of the SERS peaks at different MB concentrations corresponds roughly to the concentration ratio. However, as the thickness of gold increases the grooves disappear, the volume of nanopores, apparently, decreases, and at high concentrations of dye it can no longer be placed in pores and grooves falling under the action of capillary forces into the contact area between the spherical SiO_2 particles covered with gold. It seems so the strongest SERS hot spots are located there [10, 13], caused by plasmons localized not on the islands, but on the metal coatings of the neighboring spheres as a whole fragment, that could explain the growth of the SERS intensity with increasing gold thickness at $C = 10^{-5}$ M. It is noticeably that for the sample with gold coating thickness of $d = 34$ nm (sample 3, Table 1) the ratio of peak heights at different MB concentrations (Fig. 3) is much larger than the concentration ratio, probably, indicating different localization of molecules, namely: at $C = 10^{-6}$ M – mainly in the nanopores of the gold coating, and at $C = 10^{-5}$ M – also in the contact regions between the spheres.

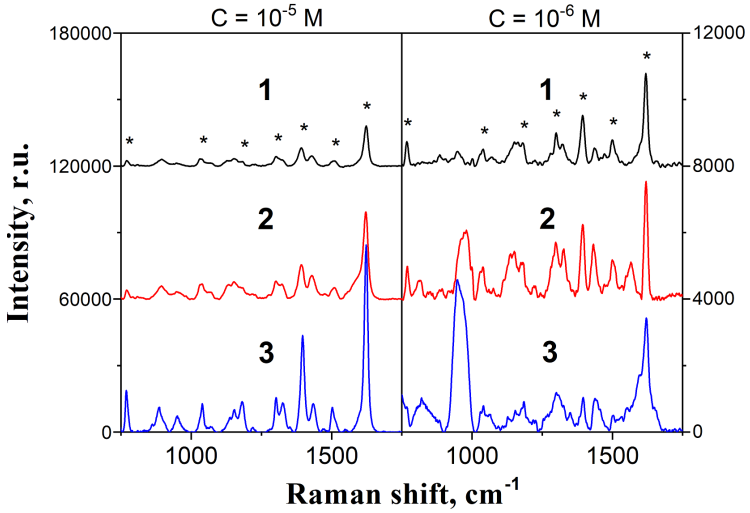

FIG. 3. SERS spectra for samples with different amounts of sputtered gold ($\lambda = 785$ nm). Concentration of MB solutions: $C = 1 \cdot 10^{-5}$ and $1 \cdot 10^{-6}$ M for the left and right panels, respectively. The curve numbers correspond to the sample numbers in Table 1. For better view, curves 1 and 2 are shifted vertically. The asterisks indicate the characteristic modes of MB

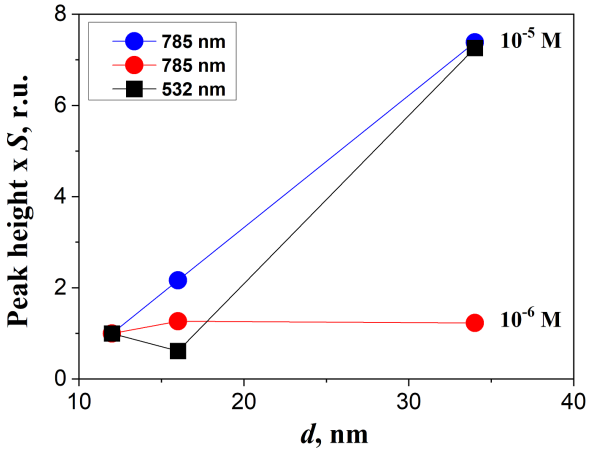

FIG. 4. Height of the main peak in SERS spectrum of MB multiplied by the surface area of the droplet S as a function of the sputtered gold thickness d. Points indicated by blue and red circles are obtained for $\lambda = 785$ nm, and black squares are obtained for $\lambda = 532$ nm. For a gold thickness of 12 nm, the peak heights are normalized to 1

When the MB concentration decreases below $C = 10^{-6}$ M the intensity of SERS maximum continues to drop rapidly. For sample 1 (Table 1) at the wavelength of incident light $\lambda = 785$ nm, we obtained a detection limit of $3 \cdot 10^{-7}$ M. At this concentration, it is still possible to sustainably detect MB in solution. In this respect, we have improved the results of Ref. [10] whose authors could not obtain for similar samples a detection limit below $1 \cdot 10^{-6}$ M even for the case when the photonic stop band coincided with the laser wavelength. Remarkable that according to Ref. [10], as the stop band approached the laser wavelength the intensity of the SERS increased several times, while the detection limit decreased by an order of magnitude. For silver-coated samples, a similar effect was reported in Ref. [12] and a weaker one in Ref. [11].

In our case, the stop-band was near 544 nm (see red arrow in Fig. 2) and the wavelength $\lambda = 532$ nm of the other laser fell on its edge. The SERS spectra collected with this laser for sample 1 (Table 1) are shown in Fig. 5. As it was shown in Ref. [17], matching the wavelength of the incident light with the stop band can give an additional enhancement of the SERS intensity by a factor of about 20. However, for our samples the electromagnetic field enhanced by Bragg reflections in the photonic crystal was weakened by the gold on the surface when leaving it. This is also evident from the height of the reflection peaks associated with the stop band, namely, for 12 nm gold it was about 11 %, for 16 nm – about 8 % (curves 1 and 2 in Fig. 2, respectively), and for 34 nm – already only about 2 % (curve 3). Accordingly, the additional enhancement due to the photonic stop-band should also decrease rapidly with a growth of gold coating thickness. For this reason, increase of the gold coating thickness from 12 to 16 nm resulted not in an increase but in a decrease of the height of the main SERS maximum for $\lambda = 532$ nm and $C = 10^{-5}$ M (see the corresponding points in Fig. 4). Further,

for $d = 34$ nm (sample 3, see Table 1), the influence of the photonic stop band effectively nullified, and a significant increase in peak height was obtained for the same reasons as for $\lambda = 785$ nm. In addition, at large d value, the intensity of the SERS modes could be further enhanced due to the approach to the laser wavelength ($\lambda = 532$ nm) of the plasmon resonance, marked in Fig. 2 by arrows. At this wavelength, we obtained for sample 1 (Table 1) the detection limit of MB $1 \cdot 10^{-6}$ M (see the lower curve in Fig. 5), which corresponds to the data of Ref. [10].

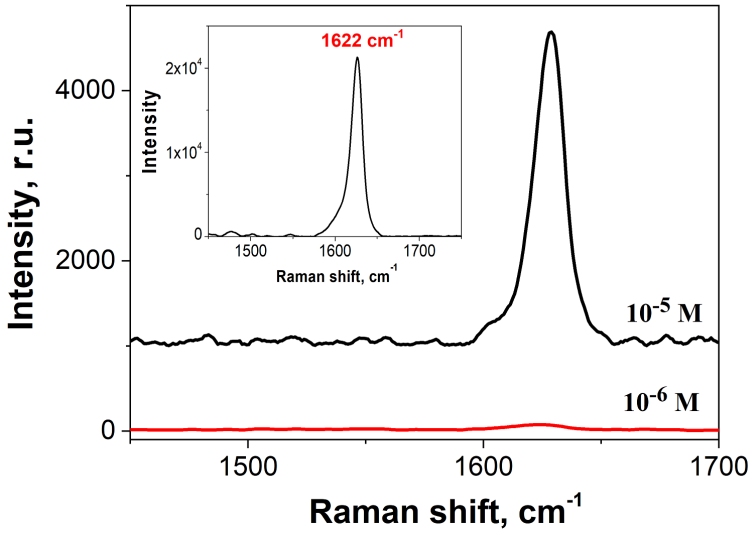

FIG. 5. Raman spectra for sample 1 (Table 1) taken at wavelength $\lambda = 532$ nm at different MB concentrations. Inset: Raman spectrum for 0.08 M of MB on a quartz glass reference sample

The *EF* of Raman scattering was determined by comparing the heights of the SERS peaks of MB deposited onto a gold-coated opal films and a reference sample of quartz glass plate, and it was calculated by the following Eq. 1 [22]:

$$EF = \frac{I_{\mathrm{SERS}}/N_{\mathrm{SERS}}}{I_0/N_0}, \tag{1}$$

where N_{SERS} and N_0 are the average number of analyte molecules in the region of SERS and reference Raman spectra collecting, respectively, and I_{SERS} and I_0 are the heights of the main peak at 1622 cm^{-1} in those and other spectra, respectively. We considered that the ratio N_{SERS}/N_0 is proportional to the ratio C/C_0 of MB concentrations in the corresponding solutions (at the reference sample $C_0 = 0.08$ M) and it is inversely proportional to the ratio of surface areas S/S_0 of the corresponding droplets (for the reference sample $S_0 = 12 \pm 1$ mm^2 – surface area of the droplet on quartz glass). The resulting formula looks as follows (Eq. 2):

$$EF = \frac{I_{\mathrm{SERS}} C_0 S}{I_0 C S_0}. \tag{2}$$

As a result, we obtained for $C = 10^{-5}$ M the *EF* values summarized in Table 1.

The dependences of the *EF* on the gold thickness d repeat the dependences shown in Fig. 4 for the height of the main SERS peak. The maximum *EF* value reached $\sim 7{\cdot}10^4$ at laser wavelength $\lambda = 785$ nm for the sample 3 ($d = 34$ nm). This value is about 1 – 2 orders of magnitude below the results reported previously for silver-coated silica opal films [11, 12]. A reasonable question arises whether the SERS intensity will increase with a further increase in d. From Table 1, we see that this is not the case: increasing d to 100 nm (sample 4) leads to a sharp drop in *EF*. Probably, the optimal thickness of gold lies in the vicinity of 40 nm. Note, that the highest SERS intensity was detected for an Ag coating with a thickness of 80 nm in [13] and only 5 nm in [12]; in both cases, a laser with a different wavelength $\lambda = 532$ nm was used.

4. Conclusions

In the present study, the issues related to gold-coated opal-type SERS substrates were addressed. It was demonstrated that at high analyte concentration $C = 10^{-5}$ M, the intensity of SERS at a wavelength of 785 nm increased with increasing amount of sputtered gold, while at $C = 10^{-6}$ M similar dependence was not observed. We believe that this is due to the complex morphology of the gold coating causing the existence of SERS hot spots of different strength. Electron microscopy has shown that at small amounts of sputtered gold, a coating with branched narrow grooves on the surface of SiO_2 spheres is obtained. At the same time, at large amounts of gold (the thickness of the gold coating on the bare glass plates above 15 nm), the upper surface of silica spheres is covered with metal completely but there are still gaps and channels between SiO_2 spheres which are not filled with gold. As a result, at concentration of the analyte MB of 10^{-6} M and at lower concentrations, as well as in case of thin island-like gold coatings, the analyte molecules fall mainly into weak

hot spots, presumably, associated with grooves and nanopores in the gold coating. Otherwise, at higher concentrations of the analyte (of $C = 10^{-5}$ M and above) and sufficient thickness of the gold coating the molecules appear in the strongest SERS hot spots in the contact areas between the SiO_2 spheres. In this case, the highest values of the SERS *EF* (see Table 1) and the best detection limits of the analyte (of about $1 \cdot 10^{-6}$ and $3 \cdot 10^{-7}$ M for $\lambda = 532$ and 785 nm, respectively) were obtained.

Despite the fact that the photonic stop band contributed to the additional enhancement of SERS signal at $\lambda = 532$ nm, this factor turned out not to be the leading one. The SERS characteristics detected with $\lambda = 785$ nm exceeded significantly both the data discussed above for $\lambda = 532$ nm and those published previously in Ref. [10]. At the same time, the fabricated samples with gold coating were inferior in enhancement factor and detection limit to similar opal materials with silver coatings [11, 12]. Despite this, they may be quite promising for practical applications due to a great thermodynamic stability of gold. The data presented in this work were collected within a year after the samples were fabricated and no particular methods of surface protection were taken, that confirms the high stability of gold-coated silica opals as promising SERS materials. To scale up the production of the proposed SERS substrates, it is desirable to replace the slow laboratory-oriented vertical deposition with a more productive process, such as the drop casting and drying method [14] or the inward-growing self-assembly [23], for example. Otherwise, our method of sputtering gold onto an opal-type layer can be easily adapted for large-scale production of efficient, reproducible and stable SERS substrates.

References

[1] Liang L., Zhao X., Wen J., Liu J., Zhang F., Guo X., Zhang K., Wang A., Gao R., Wang Y., Zhang Y. Flexible SERS Substrate with a Ag–SiO_2 Cosputtered Film for the Rapid and Convenient Detection of Thiram. *Langmuir*, 2022, **38**, P. 13753–13762.

[2] Varasteanu P., Bujor A.M., Pachiu C., Craciun G., Mihalache I., Tucureanu V., Romanitan C., Pascu R., Boldeiu A. Close-packed small nanocubes assemblies as efficient SERS substrates. *J. of Molecular Structure*, 2023, **1294**, 136441.

[3] Zha Z., Liu R., Yang W., Li C., Gao J., Shafi M., Fan X., Li Z., Du X., Jiang S. Surface-enhanced Raman scattering by the composite structure of Ag NP-multilayer Au films separated by Al2O3. *Optics Express*, 2021, **29** (6), P. 8890–8901.

[4] Cai Z., Yan Y., Liu L., Lin S., Hu X. Controllable fabrication of metallic photonic crystals for ultra-sensitive SERS and photodetectors. *RSC Adv.*, 2017, **7**, P. 55851–55858.

[5] He L., Huang J., Xu T., Chen L., Zhang K., Han S., He Y., Lee S.T. Silver nanosheet-coated inverse opal film as a highly active and uniform SERS substrate. *J. Mater. Chem.*, 2012, **22**, P. 1370–1374.

[6] Martynova N.A., Goldt A.E., Grigorieva A.V. Au-Au composites with inverse opal structure for surface-enhanced Raman spectroscopy. *Gold Bulletin*, 2018, **51**, P. 57–64.

[7] Zhu A., Zhao X., Cheng M., Chen L., Wang Y., Zhang X., Zhang Y., Zhang X. Nanohoneycomb Surface-Enhanced Raman Spectroscopy-Active Chip for the Determination of Biomarkers of Hepatocellular Carcinoma. *ACS Appl. Mater. Interfaces*, 2019, **11**, P. 44617–44623.

[8] Guo H., Qian K., Cai A., Tang J., Liu J. Ordered gold nanoparticle arrays on the tip of silver wrinkled structures for single molecule detection. *Sensors & Actuators: B. Chemical*, 2019, **300**, 126846.

[9] Ke X., Chen J., Chang L., Zhou Z., Zhang W. Casting liquid PDMS on self-assembled bilayer polystyrene nanospheres to prepare a SERS substrate with two layers of nanopits for detection of p-nitrophenol. *Anal. Methods*, 2023, **15**, P. 4582–4590.

[10] Wei M.-X., Liu C.-H., Lee H., Lee B.-W., Hsu C.-H., Lin H.-P., Wu Yu-C. Synthesis of High-Performance Photonic Crystal Film for SERS Applications via Drop-Coating Method. *Coatings*, 2020, **10**, 679.

[11] Chen G., Zhang K., Luo B., Hong W., Chen J., Chen X. Plasmonic-3D photonic crystals microchip for surface enhanced Raman spectroscopy. *Biosensors and Bioelectronics*, 2019, **143**, 111596.

[12] Chen H., Song C., Peng Z., Mao J., Zhang Y., Chen S., Zhang W., Zhang S., Zhao W., Ouyang G. The Fabrication of Photonic Crystal Microchip with Controllable Wettability and SERS Activity based on Surface Roughness for Trace Organic Compounds Determination. *Adv. Mater. Interfaces*, 2022, 2102178.

[13] Li W., Lu X., Yang R., Liang F., Chen W., Xie Z., Zheng J., Zhu J., Huang Y., Yue W., Li L., Su Y. Highly sensitive and reproducible SERS substrates with binary colloidal crystals (bCCs) based on MIM structures. *Applied Surface Science*, 2022, **597**, 153654.

[14] Dzhagan V., Mazur N., Kapush O., Skoryk M., Pirko Y., Yemets A., Dzhahan Vl., Shepeliavyi P., Valakh M., and Yukhymchuk V. Self-Organized SERS Substrates with Efficient Analyte Enrichment in the Hot Spots. *ACS Omega*, 2024, **9**, P. 4819–4830.

[15] Galisteo-Lopez J.F., Ibisate M., Sapienza R., Froufe Perez L.S., Blanco A., Lopez C. Self-Assembled Photonic Structures. *Adv. Mater.*, 2011, **23**, P. 30–69.

[16] Liu J., Zhao H., Wu M., Van der Schueren B., Yu Li, Deparis O., Ye J., Ozin G.A., Hasan T., Su B.-L. Slow Photons for Photocatalysis and Photovoltaics. *Adv. Mater.*, 2017, **29**, 1605349.

[17] Ashurov M., Abdusatorov B., Baranchikov A., Klimonsky S. Surface-enhanced Raman scattering in ETPTA inverse photonic crystals with gold nanoparticles. *Phys. Chem. Chem. Phys.*, 2021, **23**, P. 20275–20281.

[18] Jiang P., Bertone J.F., Hwang K.S., Colvin V.L. Single-Crystal Colloidal Multilayers of Controlled Thickness. *Chem. Mater.*, 1999, **11**, P. 2132–2140.

[19] Klimonsky S.O., Bakhia T., Knotko A.V., Lukashin A.V. Synthesis of Narrow_Dispersed SiO_2 Colloidal Particles and Colloidal Crystal Films Based on Them. *Doklady Chemistry,* 2014, **457** (1), P. 115–117.

[20] Stöber W., Fink A., Bohn E. Controlled Growth of Monodisperse Silica Spheres in the Micron Size Range. *J. Colloid Interface Sci.*, 1968, **26**, P. 62–69.

[21] Bakhia T., Baranchikov A.E., Gorelik V.S., Klimonsky S.O. Local Optical Spectroscopy of Opaline Photonic Crystal Films. *Crystallography Reports*, 2017, **62** (5), P. 783–786.

[22] Le Ru E., Blackie E., Meyer M., Etchegoin P.G. Surface Enhanced Raman Scattering Enhancement Factors: A Comprehensive Study. *J. Phys. Chem. C*, 2007, **111** (37), P. 13794–13803.

[23] Yan Q., Zhou Z., Zhao X.S. Inward-Growing Self-Assembly of Colloidal Crystal Films on Horizontal Substrates. *Langmuir*, 2005, **21** (7), P. 3158–3164.

Submitted 5 June 2024; revised 29 October 2024; accepted 31 October 2024

Information about the authors:

Mikhail O. Astafurov – Lomonosov Moscow State University, 119991 Leninskie gory 1, bld. 3, Moscow, Russia; mihast0707@mail.ru

Elena V. Perevedentseva – P. N. Lebedev Physical Institute of the Russian Academy of Sciences, Leninskii prospekt 53, 119991, Moscow, Russia; ORCID 0000-0002-1489-6747; perevedencevaev@lebedev.ru

Nikolay N. Melnik – P. N. Lebedev Physical Institute of the Russian Academy of Sciences, Leninskii prospekt 53, 119991, Moscow, Russia; ORCID 0000-0002-0212-9903; melniknn@lebedev.ru

Alexander E. Baranchikov – Kurnakov Institute of General and Inorganic Chemistry of the Russian Academy of Sciences, Leninskii prospekt 31, 119071, Moscow, Russia; ORCID 0000-0002-2378-7446; a.barantchikov@yandex.ru

Sergey G. Dorofeev – Lomonosov Moscow State University, 119991 Leninskie gory 1, bld. 3, Moscow, Russia; ORCID 0000-0003-3820-4853; dorofeev@inorg.chem.msu.ru

Alexander A. Ezhov – Lomonosov Moscow State University, 119991 Leninskie gory 1, bld. 3, Moscow, Russia; ORCID 0000-0001-6221-3093; alexander-ezhov@yandex.ru

Anastasia V. Grigorieva – Lomonosov Moscow State University, 119991 Leninskie gory 1, bld. 3, Moscow, Russia; ORCID 0000-0001-6102-9024; anastasia@inorg.chem.msu.ru

Sergey O. Klimonsky – Lomonosov Moscow State University, 119991 Leninskie gory 1, bld. 3, Moscow, Russia; ORCID 0000-0001-6102-1305; klimonskyso@my.msu.ru

Conflict of interest: the authors declare no conflict of interest.